

Influence of the defect structure on the refractive indices of undoped and Mg-doped lithium niobate

U. Schlarb and K. Betzler

Fachbereich Physik, Universität Osnabrück, 49069 Osnabrück, Germany

(Received 13 January 1994)

We measured the refractive indices of undoped and Mg-doped lithium niobate by an interferometric technique in a wavelength range from 400 to 1200 nm. The composition of the undoped samples varied between 47 and 50 mol% Li_2O in the crystal whereas the Mg-doped samples were grown from congruent melt with up to 9 mol% Mg. Our results can be excellently described by a generalized Sellmeier equation which takes into account the defect structure of Li-deficient and Mg-doped lithium niobate. Calculations of the phase-matching conditions of several nonlinear effects in Mg-doped lithium niobate reveal good correspondence with the respective experimental results in a temperature range from -50 to 250°C .

I. INTRODUCTION

Although lithium niobate is commonly referred to as LiNbO_3 , its phase diagram allows compositions over a range from about 45 to 50 mol% Li_2O (Ref. 1). Additionally, a variety of dopants may be added, partly up to concentrations of some 10%. One of the most interesting dopants is Mg which greatly reduces the so-called optical damage.² Both the variation of the composition and the addition of dopants strongly influence the physical properties of the material. Lithium niobate thus can be tuned to fit the requirements of a manifold of different applications.

LiNbO_3 single crystals of highest crystal quality can be grown from the congruent melt ($\approx 48.4\%$ Li_2O) by the Czochralski technique.^{3,4} The fabrication of off-congruent LiNbO_3 by this technique turns out to be difficult due to the strong composition difference between the melt and crystal.

The addition of Mg to the melt causes similar problems in the crystal growth process, usually resulting in expressed growth striations.⁵ However, newly presented improvements like the continuous charging method⁶ or the double crucible method⁷ facilitate the growth of crystals with various Li and Mg contents and good homogeneity.^{8,9} Post-growth techniques such as vapor transport equilibration¹⁰ (VTE) are also used to control the $[\text{Li}]/[\text{Nb}]$ ratio in the crystal from 47 to 49.9 mol% Li_2O in undoped¹¹ and in Mg-doped material.¹²

As doping with Mg or varying the $[\text{Li}]/[\text{Nb}]$ ratio influences not only the optical damage resistance^{2,13,14} but also the refractive indices and therefore causes strong variations in the phase-matching conditions of all nonlinear optical processes, it is of great interest to give an accurate description of the refractive indices as a function of the crystal composition. Here we present measurements of the refractive indices of LiNbO_3 in a wavelength range from 400 to 1200 nm and in a composition range from 47 to 50 mol% Li_2O for undoped and from 0 to 9 mol% Mg for doped near-congruent lithium niobate. In combination with literature data for the temperature

dependence of the refractive indices we are able to determine the parameters of a generalized Sellmeier equation which is a function of the four independent parameters wavelength, temperature, Li content, and Mg content. The generalized Sellmeier equation is used to calculate the phase-matching conditions for several nonlinear effects such as second-harmonic generation and parametric oscillation.

II. EXPERIMENTAL DETAILS

The refractive indices of LiNbO_3 and $\text{LiNbO}_3:\text{Mg}$ were measured by an interferometric technique which uses a monochromatically illuminated Michelson-type interferometer.¹⁵ In one arm of the interferometer the parallel-plate sample is rotated around an axis parallel to the c axis of the crystal and perpendicular to the incident beam, causing a rotation-angle-dependent shift in the optical path-length difference. The resulting interferogram is measured with a computer-controlled setup and is evaluated with appropriate numerical fit procedures, yielding an accuracy of about $\Delta n = 5 \times 10^{-4}$ for samples of good optical quality.^{16,17} Using a helium-neon laser tunable in the visible and infrared region or a mercury vapor lamp combined with a 0.2-m monochromator several wavelengths in the range from 400 to 1200 nm are available. Polarizing the light parallel or perpendicular to the rotation axis makes it possible to measure the extraordinary and the ordinary refractive index, respectively.

We measured six undoped LiNbO_3 samples with different $[\text{Li}]/[\text{Nb}]$ ratios varying between 46.9 to 49.9 mol% Li_2O . The crystal compositions of five crystals which had been grown by the Czochralski technique were determined from the Curie temperature measured¹⁸ yielding an accuracy of about ± 0.2 mol% Li_2O (Ref. 11). One sample was a commercially available vapor transport equilibrated crystal with approximately 49.9 mol% Li_2O (Ref. 19). The six Mg-doped samples were also grown by the Czochralski technique from a melt with an

almost congruent [Li]/[Nb] ratio of 48.5 mol% Li₂O to 51.5 mol% Nb₂O₅ and with Mg contents varying from 0 to 9 mol% Mg. The corresponding Mg content in the crystal was determined by applying the results of Hu *et al.*²⁰ who showed that the distribution coefficient of Mg changes abruptly in the region between 5 and 7 mol% from 1.2 to 0.95. The accuracy of this method is about ± 0.7 mol% Mg. The Li and Nb content in these crystals was assumed to depend on the Mg content according to a defect structure model described later.

The homogeneity of the samples was carefully checked using spatially resolved second-harmonic generation measurements.⁵ The undoped crystals revealed a homogeneity much better than the composition uncertainty.²¹ Measurements of the Mg-doped samples showed variations in the phase matching-temperature increasing from $\pm 2^\circ\text{C}$ for the undoped sample to $\pm 20^\circ\text{C}$ for a sample with 6 mol% Mg in the melt.⁵ For 9 mol% Mg the variations decreased to $\pm 6^\circ\text{C}$. This decrease might be explained by the fact that the distribution coefficient changes from 1.2 to almost unity for high doping concentrations. Attributing these variations mainly to fluctuations in the Mg content allows one to estimate that the maximum variation in the Mg content is still lower than the composition uncertainty.

The typical size after precise cutting and polishing of the samples was about $8 \times 8 \times 8 \text{ mm}^3$, well suitable for interferometric refractive index measurements.

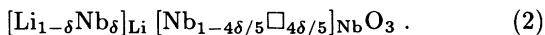
III. RESULTS AND DISCUSSION

A. Defect structure model

For a precise description of the refractive indices of undoped and Mg-doped LiNbO₃ the defect structure of the material has to be taken into account. For undoped, Li-deficient LiNbO₃ Abrahams and Marsh²² proposed a model in which each missing Li⁺ ion is replaced by a Nb⁵⁺ ion. According to their model compensating vacancies at the Nb site are created to maintain charge neutrality. Defining

$$\delta = \frac{10}{3}(50 - c_{\text{Li}})/100, \quad (1)$$

where c_{Li} denotes the [Li]/[Nb] ratio in mol% Li₂O this can be expressed by

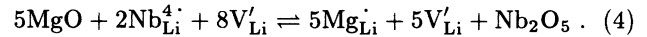


Iyi *et al.*²³ and Wilkinson *et al.*²⁴ recently suggested a different model which is also consistent with the, experimentally verified, fact that no oxygen vacancies occur. In their model the Nb sublattice remains unchanged, only one-fifth of the Li vacancies is filled with Nb antisite defects, the rest is left unoccupied to compensate for the additional charges. This can be written as



The defect structure of Mg-doped lithium niobate has

been intensively studied,^{25,26} too, and agreement is found that Mg preferably occupies Li sites and replaces Nb antisite defects up to a threshold concentration of Mg. This is described by the replacement reaction (in Kroger-Vink notation)



For Mg contents above the threshold concentration up to now none of the defect structure models under discussion is generally approved. For the quantitative description of the refractive indices in the concentration range considered here we therefore use a simplified defect structure model: Mg is only incorporated at Li sites, charge compensation takes place via Li vacancies. Neither niobium- nor oxygen-sublattice vacancies are formed. Up to a threshold concentration the number of Nb antisite defects decreases linearly with increasing Mg content according to Eq. (4). This threshold concentration c_{thr} is proportional to the respective [Li]/[Nb] ratio-dependent number of Nb antisite defects in undoped lithium niobate. Beyond the threshold no more Nb antisite defects exist, the incorporation of Mg is then governed by the replacement reaction



This simplified model is consistent with the following experimental and theoretical results

(1) Dopants in lithium niobate are found to replace only one species of cations. For Mg this is verified for concentrations up to about 10% (Ref. 20).

(2) Measurements of the optical phonon damping show that Mg does not occupy Nb sites.²⁷

(3) The distribution coefficient of Mg changes abruptly near the threshold concentration.²⁰

(4) No oxygen vacancies are found in lithium niobate.

(5) Niobium vacancies are found to be energetically very unfavorable.²⁸

(6) There is no indication in literature that by treatments like VTE lithium niobate beyond the intact niobium lattice could be fabricated.

(7) VTE-treated Mg-doped lithium niobate shows SHG phase-matching temperatures which fit excellently into this model (see Fig. 8).

B. Generalized Sellmeier equation

A description of the refractive index in terms of a Sellmeier equation consists of several oscillator terms

$$n^2 = 1 + \sum_j \frac{A_j}{\lambda_j^{-2} - \lambda^{-2}}, \quad (6)$$

where λ_j is the resonance wavelength of the j th oscillator and A_j is a parameter being proportional to the transition probability for optical excitation and the number of oscillators per volume. The various oscillators usually are regarded to be independent from each other, therefore A_j can be assumed to be proportional to the concentration

of the respective oscillator whereas λ_j should not depend on composition.

1. Nb on Nb site

Since the optical properties of LiNbO_3 in the near UV region are mainly governed by the NbO_6 octahedron,³⁰ the first oscillator term we take into account is the contribution from Nb on Nb site. Nb antisite defects or doping with Mg may influence the amount of Nb sites occupied by Nb due to vacancy creation or incorporation of Mg. The parameter A_0 therefore depends on the concentration of Nb antisite defects c_{NbLi} and the concentration of Mg c_{Mg} which can be expressed by

$$\frac{A_0}{\lambda_0^{-2} - \lambda^{-2}} [1 - F(c_{\text{NbLi}}, c_{\text{Mg}})] \quad (7)$$

as the first oscillator term. The function F must be derived from the defect structure model used, our simplified model reveals $F \equiv 0$.

2. Nb on Li site

The oscillator term describing the contribution from Nb on Li site depends linearly on the concentration of Nb_{Li} antisite defects like $A_1 c_{\text{NbLi}} / (\lambda_1^{-2} - \lambda^{-2})$. The resonance wavelengths for the Nb_{Nb} and the Nb_{Li} oscillators differ only slightly ($\lambda_0 = 223$ nm, $\lambda_1 = 260$ nm for ordinary, $\lambda_0 = 218$ nm, $\lambda_1 = 250$ nm for extraordinary polarization³¹). This can be explained by the similar octahedral configuration of Nb and Li sites in LiNbO_3 ,^{32,33} due to the nearly identical ionic radii of Nb^{5+} and Li^+ (0.69 Å and 0.68 Å, respectively). The Nb_{Li} contribution can therefore be approximated by

$$\frac{A_{\text{NbLi}} c_{\text{NbLi}}}{\lambda_0^{-2} - \lambda^{-2}}, \quad (8)$$

with $A_{\text{NbLi}} = A_1 p \approx \text{const}$, because the parameter p , defined by

$$p = \frac{\lambda_0^{-2} - \lambda^{-2}}{\lambda_1^{-2} - \lambda^{-2}}, \quad (9)$$

has only a weak wavelength dependence in the wavelength region considered here (see Fig. 1).

3. Mg on Li site

According to our simplified model Mg occupies only Li sites. The incorporation of Mg can therefore be described by an oscillator term depending linearly on the Mg content like $A_2 c_{\text{Mg}} / (\lambda_2^{-2} - \lambda^{-2})$. The ionic radius of Mg^{2+} is quite similar to that of Li^+ (0.66 Å and 0.68 Å, respectively), thus no severe lattice distortions are likely to occur which could affect the properties of the other oscillators. Absorption measurements on Mg-doped lithium niobate do not exhibit any additional absorption bands

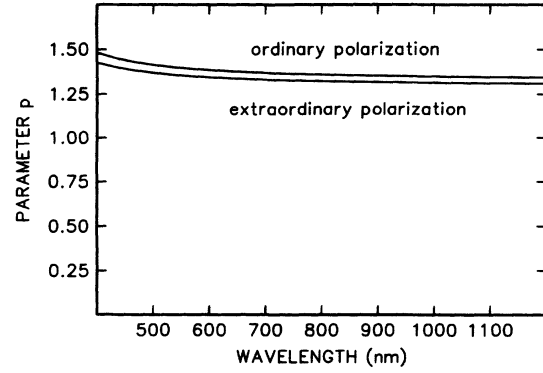


FIG. 1. Wavelength dependence of the parameter p (see text).

in the visible region, for the description of the refractive indices in the visible and near infrared region we therefore can approximate $\lambda_2 \approx \lambda_0$ in the same way as for Nb_{Li} , which leads to the Mg oscillator term

$$\frac{A_{\text{Mg}} c_{\text{Mg}}}{\lambda_0^{-2} - \lambda^{-2}}. \quad (10)$$

4. Plasmons and phonons

The contributions to the refractive index from plasmons in the far UV can be described by an oscillator term which is in good approximation independent of composition and polarization. We define

$$A_{\text{UV}} = 1 + A_3 \lambda_3^2 \quad (11)$$

as this constant UV oscillator term.

Reststrahl absorption in the IR region leads to a wavelength dependent contribution

$$-A_{\text{IR}} \lambda^2 \quad (12)$$

as the IR oscillator term.

5. The complete Sellmeier equation

The temperature dependence of the first three oscillator terms can be excellently described by a temperature dependent oscillator wavelength

$$\lambda_0(T) = \lambda_0 + \mu_0 [f(T) - f(T_0)], \quad (13)$$

where $f(T)$ is proportional to the shift of the UV absorption edge. The parameters A_{NbLi} , A_{Mg} , A_{UV} , and A_{IR} can assumed to be temperature independent (for a detailed description see Ref. 31).

All oscillator terms can be summarized to a generalized Sellmeier equation of the form

$$n_i^2 = \frac{A_{0,i}(c_{\text{Li}}, c_{\text{Mg}})}{\lambda_{0,i}(T)^{-2} - \lambda^{-2}} - A_{\text{IR},i} \lambda^2 + A_{\text{UV}}, \quad (14)$$

with

$$A_{0,i}(c_{\text{Li}}, c_{\text{Mg}}) = \begin{cases} A_{0,i} + (c_{\text{thr}} - c_{\text{Mg}})A_{\text{NbLi},i} + c_{\text{Mg}}A_{\text{Mg},i} & \text{for } c_{\text{Mg}} < c_{\text{thr}}, \\ A_{0,i} + c_{\text{Mg}}A_{\text{Mg},i} & \text{for } c_{\text{Mg}} > c_{\text{thr}}, \end{cases}$$

$$\lambda_{0,i}(T) = \lambda_{0,i} + \mu_{0,i}[f(T) - f(T_0)],$$

$$f(T) = (T + 273)^2 + 4.0238 \times 10^5 \left[\coth \left(\frac{261.6}{T + 273} \right) - 1 \right].$$

c_{thr} is a linear function of c_{Li} where c_{Li} denotes the ratio $[\text{Li}]/([\text{Nb}]+[\text{Li}])$ measured in mol% — $c_{\text{thr}} = 0\%$ for $c_{\text{Li}} = 50\%$ and $c_{\text{thr}} \approx 5\%$ for $c_{\text{Li}} = 48.5\%$, respectively. c_{Mg} is the Mg content in the crystal in mol% Mg, λ the wavelength in nm, T the temperature in °C ($T_0 = 24.5$ °C), and $i = e, o$ denotes the extraordinary and ordinary polarization, respectively.

For $c_{\text{Li}} = 50$ mol% Li_2O and $c_{\text{Mg}} = 0$ Eq. (14) is identical to expression (12) in Ref. 31. The coefficients $A_{0,i}$, $\lambda_{0,i}$, $A_{\text{IR},i}$, A_{UV} can therefore be adopted. The parameters $A_{\text{NbLi},i}$ are fitted to our measured refractive index data for undoped LiNbO_3 with varying $[\text{Li}]/[\text{Nb}]$ ratios. The measured data and the respective Sellmeier fits are shown in Fig. 2. The standard deviation is about 1.3×10^{-3} . The parameters $A_{\text{Mg},i}$ were obtained by a fit to our measurements for Mg-doped LiNbO_3 (see Fig. 3). The higher standard deviation of about 2.0×10^{-3} is mainly due to the inhomogeneity of the samples. However, the birefringence we calculated from the generalized Sellmeier equation in Fig. 4 is in good correspondence with our experimental data.

Finally the parameters $\mu_{0,i}$ for the temperature dependence of the refractive indices are fitted to temperature dependent literature data for congruent³⁵ and stoichiometric¹⁹ LiNbO_3 . Figure 5 shows that in spite of the parameters $\mu_{0,i}$ being fitted to undoped LiNbO_3 the generalized Sellmeier equation also gives an excellent description of the temperature dependence of the refractive indices for Mg-doped LiNbO_3 . Doping with Mg has therefore no significant influence on the temperature dependence of the refractive index. The numerical results for all parameters are given in Table I.

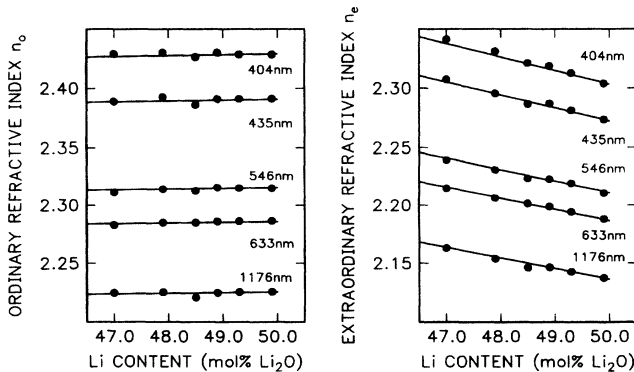


FIG. 2. Dependence of the ordinary (n_o) and extraordinary (n_e) refractive index of undoped LiNbO_3 on the Li content for various wavelengths at room temperature. The curves are calculated from the generalized Sellmeier equation (see text).

C. Nonlinear effects in Mg-doped lithium niobate

The phase-matching parameters of all nonlinear effects can be calculated from the conditions for energy and momentum conservation. For undoped LiNbO_3 ,^{31,36} we found excellent correspondence with the respective experimental results of several authors. Moreover, for $c_{\text{Mg}} = 0$ the generalized Sellmeier equation allows one to calculate the calibration curves for all refractive-index-dependent characterization techniques which are used to determine the $[\text{Li}]/[\text{Nb}]$ ratio in undoped LiNbO_3 .³⁷ Here we will concentrate on nonlinear effects in Mg-doped LiNbO_3 .

1. Noncolinear frequency doubling

In the technique of spontaneous noncolinear frequency doubling (SNCFD) first presented by Giordmaine³⁹ the vectorial phase-matching condition must be obeyed by an ordinary polarized intense laser beam (\mathbf{k}_1), its Rayleigh scattered light (\mathbf{k}_2), and the extraordinary polarized second-harmonic light ($\mathbf{k}_3 = \mathbf{k}_1 + \mathbf{k}_2$) which forms an elliptic cone around the incident beam. In a plane normal to the optic axis the cone angle φ_{cryst} between the second-harmonic light and the incident beam is defined by^{40,41}

$$\cos \varphi_{\text{cryst}} = n_e(\lambda_1/2)/n_o(\lambda_1). \quad (15)$$

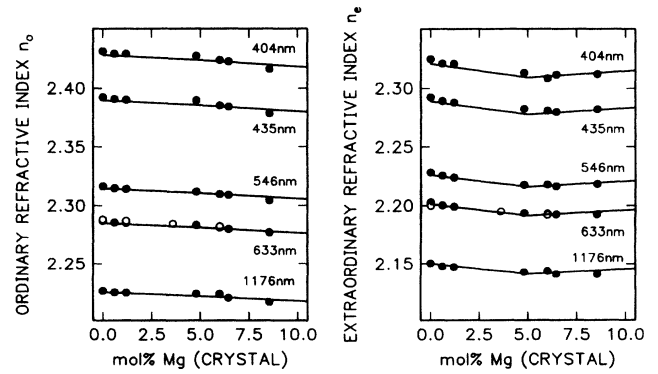


FIG. 3. Dependence of the ordinary (n_o) and extraordinary (n_e) refractive index of Mg-doped LiNbO_3 grown from congruent melt on the Mg content in the crystal for various wavelengths at room temperature. Filled circles refer to our measurements, open circles are measurements by Furukawa *et al.* (Ref. 29). The curves are calculated from the generalized Sellmeier equation (see text).

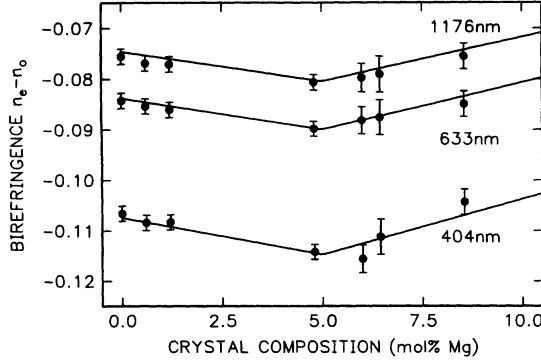


FIG. 4. Dependence of the birefringence of Mg-doped LiNbO₃ grown from congruent melt on the Mg content in the crystal for various wavelengths at room temperature. The curves are calculated from the generalized Sellmeier equation (see text).

Applying the Snellius law one obtains the respective angle φ_{air} outside the crystal. In Fig. 6 the computed cone angle φ_{air} is depicted as a function of the Mg content in the crystal for a fundamental wavelength of 1064 nm, $c_{\text{Li}} = 48.5$ mol % Li₂O and $T = 24.5$ °C. For $c_{\text{Mg}} = 8.5$ mol % Mg the cone angle converges to $\varphi_{\text{air}} = 0^\circ$, which means that colinear frequency doubling at room temperature is observed. Since the [Li]/[Nb] ratio in the crystal may be influenced by the Mg doping,⁴² we also calculated the phase-matching conditions for slightly different Li contents. Within a variation of ± 0.2 mol % Li₂O there is good correspondence with our measurements and the result of Volk *et al.* (Ref. 38). Figure 6 shows that in our simple model a variation of the Li content for $c_{\text{Mg}} > c_{\text{thr}}$ has no effect on the SNCFD angle because all Nb antisite defects are already replaced by Mg [Eq. (4)].

2. Angle phase matching

The phase-matching condition for type-I angle phase-matching in LiNbO₃ can be written as

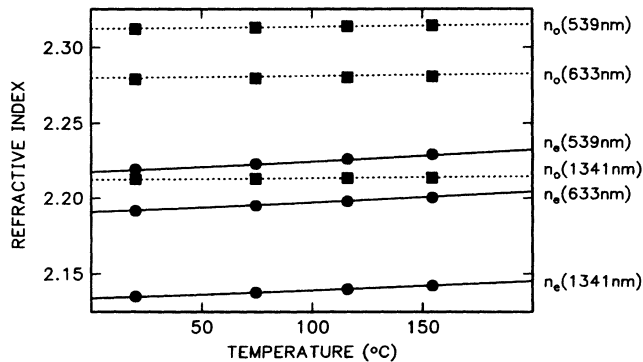


FIG. 5. Temperature dependence of the refractive indices of LiNbO₃ grown from congruent melt doped with 5 mol % Mg (about 6 mol % Mg in the crystal) for various wavelengths. The curves are calculated from the generalized Sellmeier equation (see text). Data points correspond to experimental results from Shen *et al.* (Ref. 34).

TABLE I. Parameters of the generalized Sellmeier equation. For the definition see Eq. (14) in the text.

n_o		n_e	
$\lambda_{0,o} = 223.219$		$\lambda_{0,e} = 218.203$	
$\mu_{0,o} = 1.1082 \times 10^{-6}$		$\mu_{0,e} = 6.4047 \times 10^{-6}$	
$A_{0,o} = 4.5312 \times 10^{-5}$		$A_{0,e} = 3.9466 \times 10^{-5}$	
$A_{\text{NbLi},o} = -1.4464 \times 10^{-8}$		$A_{\text{NbLi},e} = 2.3727 \times 10^{-7}$	
$A_{\text{Mg},o} = -7.3548 \times 10^{-8}$		$A_{\text{Mg},e} = 7.6243 \times 10^{-8}$	
$A_{\text{IR},o} = 3.6340 \times 10^{-8}$		$A_{\text{IR},e} = 3.0998 \times 10^{-8}$	
$A_{\text{UV}} = 2.6613$		$A_{\text{UV}} = 2.6613$	

$$\frac{1}{n_o^2(\lambda_1)} = \frac{\cos^2 \theta}{n_o^2(\lambda_1/2)} + \frac{\sin^2 \theta}{n_e^2(\lambda_1/2)}, \quad (16)$$

where θ denotes the direction of propagation in the crystal with respect to the optic axis. In Fig. 7 the phase-matching angle is computed as a function of the crystal composition for $T = 24.5$ °C and two fundamental wavelengths λ_1 . Our experimental data and the results from other authors^{43,34} agree well with our calculations within an uncertainty in the [Li]/[Nb] ratio of ± 0.3 mol % Li₂O.

3. Phase-matching temperature

The phase matching condition for colinear noncritical type-I second-harmonic generation (SHG) is equivalent to

$$\Delta n_{\text{SHG}} = n_e(\lambda_1/2, T_{\text{PM}}) - n_o(\lambda_1, T_{\text{PM}}) = 0, \quad (17)$$

which allows one for a given Li and Mg content to compute the phase-matching (PM) temperature T_{PM} (see Fig. 8). Our calculations for LiNbO₃:Mg crystals grown

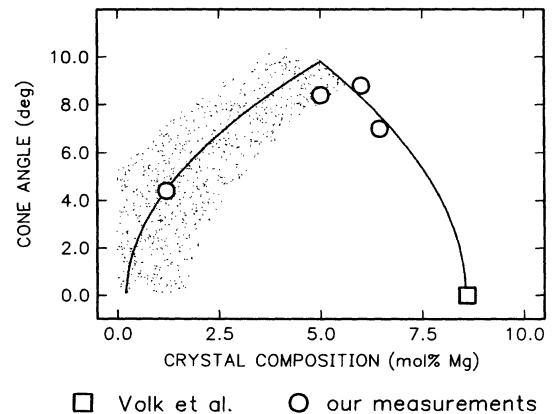


FIG. 6. Cone angle for spontaneous noncolinear frequency doubling as a function of the Mg content in the crystal. The curve is calculated from the generalized Sellmeier equation (see text) for a fundamental wavelength of 1064 nm and $T = 24.5$ °C. The data points represent our measurements and the result of Volk *et al.* (Ref. 38). The angles are measured outside the crystal in a plane normal to the optic axis. The grey shaded area corresponds to a variation in the [Li]/[Nb] ratio of the crystal of 48.5 ± 0.2 mol % Li₂O.

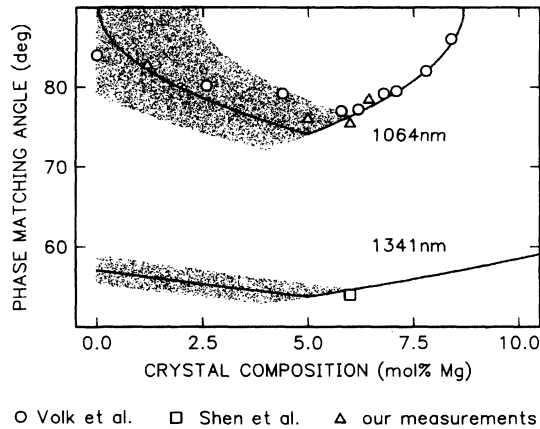


FIG. 7. Phase-matching angle as a function of the crystal composition. The angles are measured inside the crystal with respect to the optic axis. The curves are calculated from the generalized Sellmeier equation (see text). The grey shaded area corresponds to a variation in the $[Li]/[Nb]$ ratio of the crystal of 48.5 ± 0.3 mol% Li_2O . Data points represent our measurements and results of Volk *et al.* (Ref. 43) and Shen *et al.* (Ref. 34).

from almost congruent melt agree well with the experimental results from Schmidt *et al.*⁵ and Volk *et al.*³⁸ For $c_{Mg} < c_{thr}$ the deviations of the experimental values from the calculated curve can be explained by a variation of the Li content by ± 0.2 mol% Li_2O . For $c_{Mg} > c_{thr}$ the additional error in the Mg content has to be taken into account, which explains, for example, the discrepancy in the literature values for 8.5 mol% Mg.

Moreover, the composition dependence of the phase-matching temperature for vapor transport equilibrated

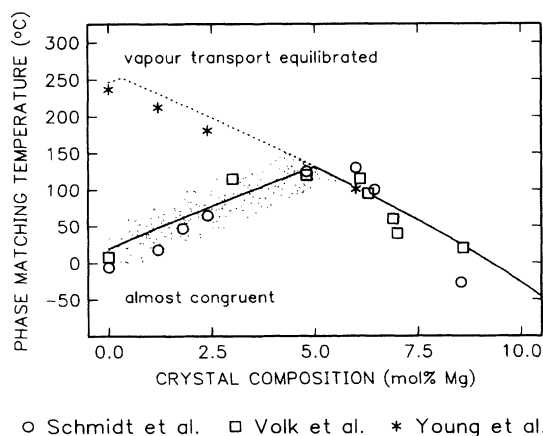


FIG. 8. Phase-matching temperature of $LiNbO_3:Mg$ as a function of the Mg content in the crystal for a fundamental wavelength of 1064 nm. The curves are calculated from the generalized Sellmeier equation (see text) for a $[Li]/[Nb]$ ratio of 48.5 ± 0.2 mol% Li_2O (almost congruent, solid line, and grey shaded area) and 49.9 mol% Li_2O (vapor transport equilibrated, dotted curve). The data points show results from Schmidt *et al.* (Ref. 5), Volk *et al.* (Ref. 38), and Young *et al.* (Ref. 12).

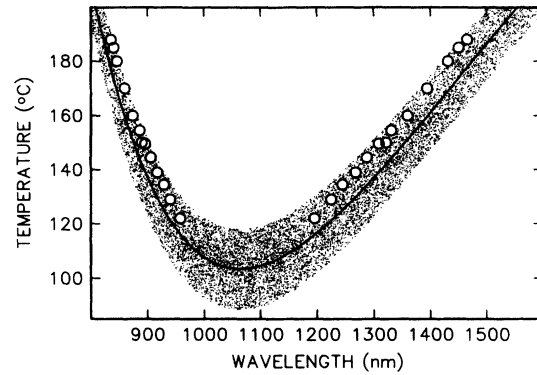


FIG. 9. Phase-matching temperatures for parametric oscillation in $LiNbO_3:Mg$ grown from almost congruent melt (48.6 mol% Li_2O) with 5 mol% Mg in the melt (about 6 mol% Mg in the crystal) as a function of the signal and idler wavelength. The curve is calculated from the generalized Sellmeier equation for a pump wavelength of 532 nm. The grey shaded area corresponds to a variation in the Mg content of ± 0.5 mol% Mg. Data points correspond to experimental results from Kozlovsky *et al.* (Ref. 44).

(VTE) material¹² can be explained. Below the threshold value a VTE treatment decreases the amount of Nb anti-site defects because $c_{Li} \approx 50$ mol% Li_2O , which leads to an increase in the phase-matching temperature. Above c_{thr} all Nb anti-site defects are already replaced by the Mg doping [Eq. 4]. An additional VTE treatment has no significant effect on the phase-matching temperature.

Assuming $\partial n_e(532 \text{ nm})/\partial T \approx 1 \times 10^{-4}/^\circ C$ and neglecting $\partial n_o(1064 \text{ nm})/\partial T$ the maximum error in the calculated refractive index can be estimated. With $\Delta T_{PM} = 20^\circ C$ this leads to $\Delta n = 0.002$ which is in good correspondence with the fit accuracy.

4. Parametric oscillation and difference frequency mixing

For a $LiNbO_3:Mg$ crystal grown from almost congruent melt (48.6 mol% Li_2O) with 5 mol% Mg (corresponding to about 6 mol% Mg in the crystal) we calculated the phase-matching temperatures of parametric oscillation (Fig. 9). Within a variation in the Mg content of ± 0.5 mol% Mg there is good agreement with the respective experimental values of Kozlovsky *et al.*⁴⁴ even in the IR region from 1200 to 1500 nm.

IV. CONCLUSION

We propose a generalized Sellmeier equation which describes the refractive indices of $LiNbO_3$ and $LiNbO_3:Mg$ as a function of composition, wavelength, and temperature. The equation consists of several oscillator terms representing approximated infrared and plasmonic contributions and a summarized term for Mg and Nb on a Nb or Li site. The temperature variation is assumed to be proportional to the shift of the UV absorption edge

with temperature. The parameters of this equation were fitted to our refractive index measurements for undoped and Mg-doped LiNbO₃ and literature data.

The generalized Sellmeier equation allows one to calculate all refractive-index-dependent effects in undoped and Mg-doped LiNbO₃ with excellent accuracy. Calculations of nonlinear effects like second-harmonic generation and parametric oscillation in LiNbO₃:Mg verify that the equation gives an accurate description of the refractive indices in the composition range from 0 to 9 mol% Mg, in the wavelength range from 400 to at least 1200 nm and for temperatures between -50 and at least 250 °C.

Effects of a variation in the [Li]/[Nb] ratio are also described correctly. The maximum error in the calculated refractive indices is about 0.002.

ACKNOWLEDGMENTS

We are greatly indebted to B. C. Grabmaier for the growth and precise characterization of the sample crystals. Financial support from the Deutsche Forschungsgemeinschaft (SFB 225) is gratefully acknowledged.

- ¹ J. G. Bergman *et al.*, *Appl. Phys. Lett.* **12**, 92 (1968).
- ² D. A. Bryan, R. Gerson, and H. E. Tomaschke, *Appl. Phys. Lett.* **44**, 847 (1984).
- ³ R. L. Byer, J. F. Young, and R. S. Feigelson, *J. Appl. Phys.* **41**, 2320 (1970).
- ⁴ P. F. Bordui, R. G. Norwood, C. D. Bird, and G. D. Calvert, *J. Cryst. Growth* **113**, 61 (1991).
- ⁵ N. Schmidt, K. Betzler, and S. Kapphan, *Cryst. Lattice Defects Amorph. Mater.* **15**, 103 (1987).
- ⁶ S.-J. Kan *et al.*, *J. Cryst. Growth* **119**, 215 (1992).
- ⁷ K. Kitamura *et al.*, *J. Cryst. Growth* **116**, 327 (1992).
- ⁸ Y. Furukawa, M. Sato, K. Kitamura, and F. Nitanda, *J. Cryst. Growth* **128**, 909 (1993).
- ⁹ S. Kan *et al.*, *J. Cryst. Growth* **128**, 915 (1993).
- ¹⁰ R. L. Holman, *Mater. Sci. Res.* **11**, 343 (1978).
- ¹¹ P. F. Bordui, R. G. Norwood, D. H. Jundt, and M. M. Fejer, *J. Appl. Phys.* **71**, 875 (1992).
- ¹² W. M. Young, R. S. Feigelson, D. H. Jundt, and M. M. Fejer, *J. Appl. Phys.* **69**, 7372 (1991).
- ¹³ Y. Furukawa *et al.*, *J. Appl. Phys.* **72**, 3250 (1992).
- ¹⁴ G. I. Malovichko *et al.*, *Appl. Phys. A* **56**, 103 (1993).
- ¹⁵ M. S. Shumate, *Appl. Opt.* **5**, 327 (1966).
- ¹⁶ K. Betzler, A. Gröne, N. Schmidt, and P. Voigt, *Rev. Sci. Instrum.* **59**, 652 (1988).
- ¹⁷ U. Schlarb and K. Betzler, *Ferroelectrics* **126**, 39 (1992).
- ¹⁸ B. C. Grabmaier, W. Wersing, and W. Koestler, *J. Cryst. Growth* **110**, 339 (1991).
- ¹⁹ D. H. Jundt, M. M. Fejer, and R. L. Byer, *IEEE J. Quantum Electron.* **QE-26**, 135 (1990).
- ²⁰ L. J. Hu, Y. H. Chang, I. N. Lin, and S. J. Yang, *J. Cryst. Growth* **114**, 191 (1991).
- ²¹ N. Schmidt, K. Betzler, and B. C. Grabmaier, *Appl. Phys. Lett.* **58**, 34 (1991).
- ²² S. C. Abrahams and P. Marsh, *Acta Crystallogr. B* **42**, 61 (1986).
- ²³ N. Iyi *et al.*, *J. Solid State Chem.* **101**, 340 (1992).
- ²⁴ A. P. Wilkinson, A. K. Cheetham, and R. H. Jarman, *J. Appl. Phys.* **74**, 3080 (1993).
- ²⁵ Z. Qiren and F. Xiqi, *Phys. Rev. B* **43**, 12019 (1991).
- ²⁶ H. Donnerberg, S. M. Tomlinson, C. R. A. Catlow, and O. F. Schirmer, *Phys. Rev. B* **44**, 4877 (1991).
- ²⁷ S. Kojima, *Jpn. J. Appl. Phys.* **32**, 4373 (1993).
- ²⁸ H. Donnerberg, S. M. Tomlinson, C. R. A. Catlow, and O. F. Schirmer, *Phys. Rev. B* **40**, 11909 (1989).
- ²⁹ Y. Furukawa, M. Sato, F. Nitanda, and K. Ito, *J. Cryst. Growth* **99**, 832 (1990).
- ³⁰ E. Wiesendanger and G. Güntherodt, *Solid State Commun.* **14**, 303 (1974).
- ³¹ U. Schlarb and K. Betzler, *Phys. Rev. B* **48**, 15613 (1993).
- ³² D. M. Smyth, *Ferroelectrics* **50**, 419 (1983).
- ³³ A. Mehta, A. Navrotsky, N. Kumada, and N. Kinomura, *J. Solid State Chem.* **102**, 213 (1993).
- ³⁴ H. Y. Shen *et al.*, *Appl. Opt.* **31**, 6695 (1992).
- ³⁵ G. J. Edwards and M. Lawrence, *Opt. Quantum Electron.* **16**, 373 (1984).
- ³⁶ U. Schlarb and K. Betzler, *Ferroelectrics* (to be published).
- ³⁷ U. Schlarb and K. Betzler, *J. Appl. Phys.* **73**, 3472 (1993).
- ³⁸ T. R. Volk and N. M. Rubinina, *Fiz. Tverd. Tela (Leningrad)* **33**, 1192 (1991) [*Sov. Phys. Solid State* **33**, 674 (1991)].
- ³⁹ J. A. Giordmaine, *Phys. Rev. Lett.* **8**, 19 (1962).
- ⁴⁰ H. E. Bates, *J. Opt. Soc. Am.* **61**, 904 (1971).
- ⁴¹ A. Reichert and K. Betzler, *Ferroelectrics* **126**, 9 (1992).
- ⁴² Z. Yanfei *et al.*, *J. Cryst. Growth* **114**, 87 (1991).
- ⁴³ T. R. Volk *et al.*, *Ferroelectrics* **109**, 345 (1990).
- ⁴⁴ W. J. Kozlovsky, E. K. Gustafson, R. C. Eckardt, and R. Byer, *Opt. Lett.* **13**, 1102 (1988).

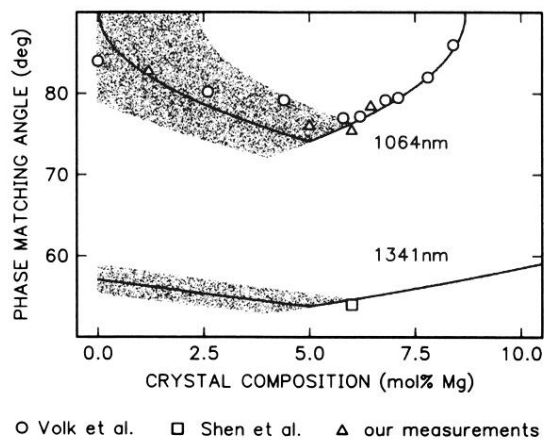
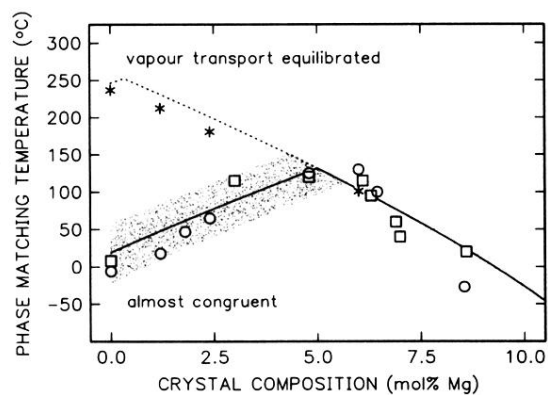


FIG. 7. Phase-matching angle as a function of the crystal composition. The angles are measured inside the crystal with respect to the optic axis. The curves are calculated from the generalized Sellmeier equation (see text). The grey shaded area corresponds to a variation in the [Li]/[Nb] ratio of the crystal of 48.5 ± 0.3 mol% Li_2O . Data points represent our measurements and results of Volk *et al.* (Ref. 43) and Shen *et al.* (Ref. 34).



○ Schmidt et al. □ Volk et al. * Young et al.

FIG. 8. Phase-matching temperature of $\text{LiNbO}_3:\text{Mg}$ as a function of the Mg content in the crystal for a fundamental wavelength of 1064 nm. The curves are calculated from the generalized Sellmeier equation (see text) for a $[\text{Li}]/[\text{Nb}]$ ratio of 48.5 ± 0.2 mol% Li_2O (almost congruent, solid line, and grey shaded area) and 49.9 mol% Li_2O (vapor transport equilibrated, dotted curve). The data points show results from Schmidt *et al.* (Ref. 5), Volk *et al.* (Ref. 38), and Young *et al.* (Ref. 12).

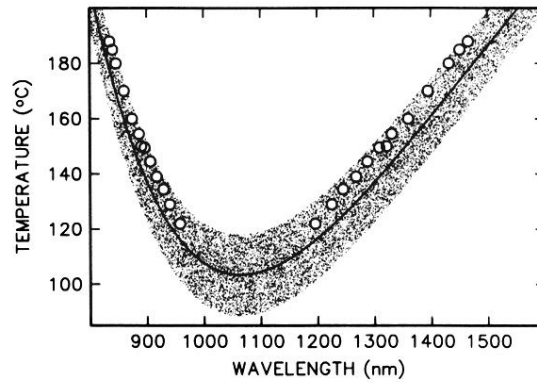


FIG. 9. Phase-matching temperatures for parametric oscillation in $\text{LiNbO}_3\text{:Mg}$ grown from almost congruent melt (48.6 mol % Li_2O) with 5 mol % Mg in the melt (about 6 mol % Mg in the crystal) as a function of the signal and idler wavelength. The curve is calculated from the generalized Sellmeier equation for a pump wavelength of 532 nm. The grey shaded area corresponds to a variation in the Mg content of ± 0.5 mol % Mg. Data points correspond to experimental results from Kozlovsky *et al.* (Ref. 44).